

# Automatic Parameter Estimation for Graph-Cut Chan-Vese for Fluorescence Image Binarization

Ryan Naidoo, Jules-Raymond Tapamo

## Abstract

The detailed analytical studies of microscopic organisms and such have played a vital role in a host of fields ranging from the simple curiosity of what goes on at the micro-level to studying the behaviour of cancerous cells. Fluorescence images are generated by the thousands to study these phenomena. The rate at which we're able to gather data outweighs the rate at which we're able to accurately study it. The purpose of this study is to investigate the properties of fluorescence images and leverage that understanding to develop a technique that is able to automatically produce image-specific accurate parameter settings for segmentation of the object of interest. In this paper, we present a novel parameter estimation technique for the graph cut implementation of the Chan-Vese approximation of the Mumford-Shah functional for image segmentation. The effectiveness of the technique is demonstrated through a set of experiments with real images. We pit our approach against two other common parameter settings. Our segmentation scheme is highly robust and produces superior segmentation results with an average accuracy of 93.533%.

## Keywords

*Image segmentation, graph cuts, fluorescence, active-contours, Chan-Vese, Mumford-Shah.*

## I. INTRODUCTION

**Lay the foundation to present the problem.** Amount of images. Problems with the images. The type of solutions available that miss solving the problem. **Present the problem. What solution do we seek. Scope of the paper. Other tried approaches. What are their weaknesses? What did they sacrifice to get that scheme or result. What schemes will we be competing with. Organisation.** Firstly, we begin in Section II with a brief introduction to the Chan-Vese formulation of the Mumford-Shah energy functional. Then in Section III we introduce the graph-cut approach to image segmentation and how it is used to solve the Chan-Vese image segmentation problem. We then develop the proposed technique for parameter estimation in Section IV. In Section V we show some experimental results and demonstrate the efficiency and robustness of this scheme. We also compare the proposed scheme against two other well-known schemes. Our concluding remarks are shown in Section VI.

## II. CHAN-VESE FORMULATION OF THE MUMFORD-SHAH ENERGY FUNCTIONAL

The Mumford-Shah evolution energy functional is a segmentation model to be minimised over an approximation image  $u$  of the input image  $u_0$ . The level set representation of the Mumford-Shah energy function is

$$\begin{aligned} F(c_1, c_2, \phi) = & \mu \int_{\Omega} \delta(\phi(x, y)) |\nabla \phi(x, y)| dx dy \\ & + \nu \int_{\Omega} H(\phi(x, y)) dx dy \\ & + \lambda_1 \int_{\Omega} |u(x, y) - c_1|^2 H(\phi(x, y)) dx dy \\ & + \lambda_2 \int_{\Omega} |u(x, y) - c_2|^2 (1 - H(\phi(x, y))) dx dy, \end{aligned} \quad (1)$$

where  $\lambda_1, \lambda_2, \mu$ , and  $\nu$  are fixed parameters such that  $\lambda_1, \lambda_2 > 0$  and  $\mu, \nu \geq 0$ .  $u(x, y)$  is the image,  $H(\cdot)$  is the Heaviside step function,  $\delta(\cdot)$  is the Dirac delta function,  $\Phi$  is an open unbounded subset of  $\mathbb{R}^2$  and  $\phi : \Omega \rightarrow \mathbb{R}$  is the level set function, such that:

$$\begin{aligned} \omega &= \{(x, y) \in \Omega | \Phi(x_p) > 0\} \\ \bar{\omega} &= \{(x, y) \in \Omega | \Phi(x_p) < 0\} \\ C &= \partial\omega = \{(x, y) \in \Omega | \Phi(x_p) = 0\}, \end{aligned} \quad (2)$$

$c_1$  and  $c_2$  are the arithmetic means of the intensities in the regions of  $u$  defined by the masks  $H(\phi(x, y))$  and  $1 - H(\phi(x, y))$  respectively. The piece-wise smooth approximation of the image is then

$$u(x, y) = c_1 H(\phi(x, y)) + c_2 (1 - H(\phi(x, y))). \quad (3)$$

### A. Discretising the Mumford-Shah Functional

With the exception of the second term in Equation (1), the remaining terms can be represented discretely very easily. For each pixel  $p \in \Omega$ , let  $x_p$  be a binary variable such that

$$x_p = \begin{cases} 0 & \phi(p) \leq 0 \\ 1 & \phi(p) > 0 \end{cases} \quad (4)$$

The means can now be calculated using

$$c_1 = \frac{\sum_p u(x, y) x_p}{\sum_p x_p}, \quad (5)$$

$$c_2 = \frac{\sum_p u(x, y) (1 - x_p)}{\sum_p (1 - x_p)}. \quad (6)$$

For simplification, set  $\nu = 0$ . Kolmogorov and Boykov in [] used the Cauchy-Crofton theorem to approximate the length of a contour  $C$  by counting the number of intersections with the line  $L$ . By using this approximation, it can be shown that the Euclidean contour length can be expressed as

$$\|C\|_E = \sum_{p, q \in e_k} w_k(x_p(1 - x_q) + x_q(1 - x_p)). \quad (7)$$

The fully discrete form of Equation (1) is

$$\begin{aligned}
 F(x_1, \dots, x_n) = & \mu \sum_{p,q \in e_k} w_k(x_p(1-x_q) + x_q(1-x_p)) \\
 & + \lambda_1 \sum_p |u(x, y) - c_1|^2 x_p \\
 & + \lambda_2 \sum_p |u(x, y) - c_2|^2 (1-x_p)
 \end{aligned} \tag{8}$$

### III. GRAPH-CUT MODEL FOR CHAN-VESE SEGMENTATION

Graph Cuts are a well known optimisation problem in Combinatorics. Due to the duality known as the Max-Flow Min-Cut Theorem, there are several fast algorithms to find the mincut. Typically, it's easier to solve the Max-Flow problem and bulk of the optimised algorithms are designed on Max-flow algorithms. Graph Cuts were unsuccessfully introduced into Computer Vision by Greig *et al.* [] and was later popularised by Kolmogorov [].

A graph  $G = (V, E)$  is a set of vertices/nodes  $V$ , and a set of directed edges  $E$  with positive weights/capacities that connect these vertices. We let  $uv$  be a directed edge going from  $u$  to  $v$ . The weight of the edge is denoted by  $c(u, v)$ . In the 2-label graph cut, there are two more vertices that don't correspond to any pixels. These are the source  $s$  and the sink  $t$ . All other nodes are directly connected to both the source and the sink. Therefore, a cut on  $G$  is a partitioning of  $V$  into two disjoint connected sets  $(V_s, V_t)$  such that  $s \in V_s$  and  $t \in V_t$ . The cost of the cut is calculated as

$$c(V_s, V_t) = \sum_{i \in V_s, j \in V_t} c(i, j). \tag{9}$$

Graph cuts are used to minimise energies of the form

$$\arg \min_{x \in \{0,1\}^m} E(x) = \sum_i E^i(x_i) + \sum_{i < j} E^{i,j}(x_i, x_j). \tag{10}$$

For an energy to be graph-representable, the pairwise interaction potentials must be submodular [], i.e. it must adhere to the following constraint.

$$E^{i,j}(0, 0) + E^{i,j}(1, 1) \leq E^{i,j}(0, 1) + E^{i,j}(1, 0), \forall i < j. \tag{11}$$

It has been shown in [] that Equation (8) is submodular and hence the optimal solution can be found via graph cuts. The data and regularisation energy respectively in Equation (10) is

$$E^i(x_i) = \lambda_1 |u(x, y) - c_1|^2 x_i + \lambda_2 |u(x, y) - c_2|^2 (1 - x_i) \tag{12}$$

$$E^{i,j}(x_i, x_j) = (x_i + x_j - 2x_i x_j) w_{ij} \tag{13}$$

### IV. CHAN-VESE PARAMETER ESTIMATION FOR GRAPH-CUTS

In this section we introduce the proposed method for Chan-Vese parameter estimation for graph-cuts. Previous parameter estimation schemes focussed on a certain genre of images or image characteristics, and these resulted in a set of hard-coded parameter settings. These hard-coded parameters are not very useful in producing consistent results in the greater applications of image segmentation even within the fields for which they were optimised.

We devise a novel weighting scheme for the graph and propose a general parameter estimation technique in which the parameters adapt themselves to the image. We achieve this not by focusing on the parameters, but rather the relationship between the parameters. We then isolate these relationships in proxy relational parameters which we then tune for fluorescence images.

#### A. Proposed Technique

We first explain the method used to weight the graph. We begin by normalising the data and smoothing connections. We use the Euclidean distance to weighting of the edges connecting adjacent nodes, i.e. diagonally adjacent node in the 8-connected graph would be scaled by  $\frac{1}{\sqrt{2}}$ , etc.

The image pixel values are also normalised i.e.  $p \in [0, 1]$ , where  $p$  is the pixel value of the  $i$ -th pixel in the image. The edge connecting the source to the node which corresponds to pixel  $i$  is given by  $E^i(0)|_{i=p} = \lambda_0|p - c_0|^2$ . This is how far away the pixel is from the average foreground/object pixel intensity  $c_0$ . Similarly, the weight of the connection from the node to the sink is given by  $E^i(1)|_{i=p} = \lambda_1|p - c_1|^2$ , i.e. how far away the pixel is from the average background pixel intensity  $c_1$ .

Whether a node is connected to the source or the sink after segmentation depends on its connections which are weighted by the previously defined energy functions. It behooves use to study then, the relationship between the energy functions. We see that there are two tunable parameters namely  $\lambda_0$  and  $\lambda_1$ . It is the relationship between these two parameter that heavily influence the output. We simplify and explicitly formalise the relationship between and set

$$\lambda_0 = \alpha\lambda_1. \quad (14)$$

Forcing this relationship make further analysis simpler and more intuitive. An immediate constraint is  $\alpha > 0$ , since we require all data connections to be positive, i.e.  $E^i(0), E^i(1) \geq 0$ .

We will now analyse the flow through a single node in the 8-connected graph, we use Figure 1 to facilitate our explanation. Two nodes are maximally connected if their corresponding pixel values are the same, i.e. there is no difference between them. Let this value be  $\mu$ . Hence, the maximum possible flow into or out of a node to its neighbours is

$$f_{max} = 4\mu + 4\frac{\mu}{\sqrt{2}} = \mu(2\sqrt{2} + 4). \quad (15)$$

We know that for a node  $p$  to belong to the source set, i.e.  $p \in S$ , the incoming flow from the source must completely saturate all outlets. This can be expressed as

$$E^i(0) > E^i(1) + \mu(2\sqrt{2} + 4). \quad (16)$$

Similarly, to guarantee the node will be in the sink set,  $p \in T$ , we have

$$E^i(1) > E^i(0) + \mu(2\sqrt{2} + 4). \quad (17)$$

To aid in understanding the energies, we use Figure 2.

For quadratic energies with  $0 < c_0 < c_1 < 1$ , there is a point, between  $c_0$  and  $c_1$ , where the incoming flow from the source completely saturates the sink with no excess remaining. This point, where the energies are equal,

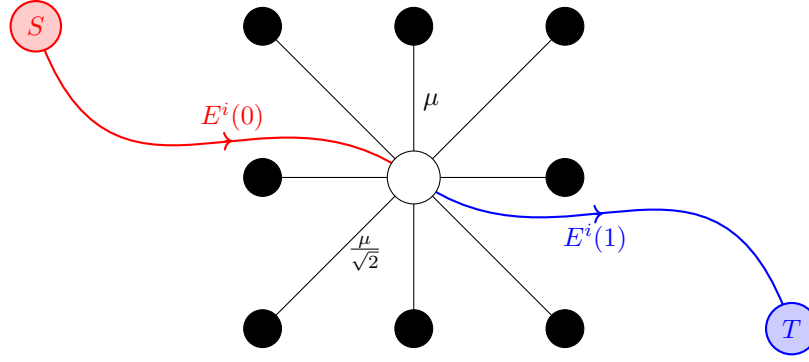


Fig. 1. Fully connected single node.

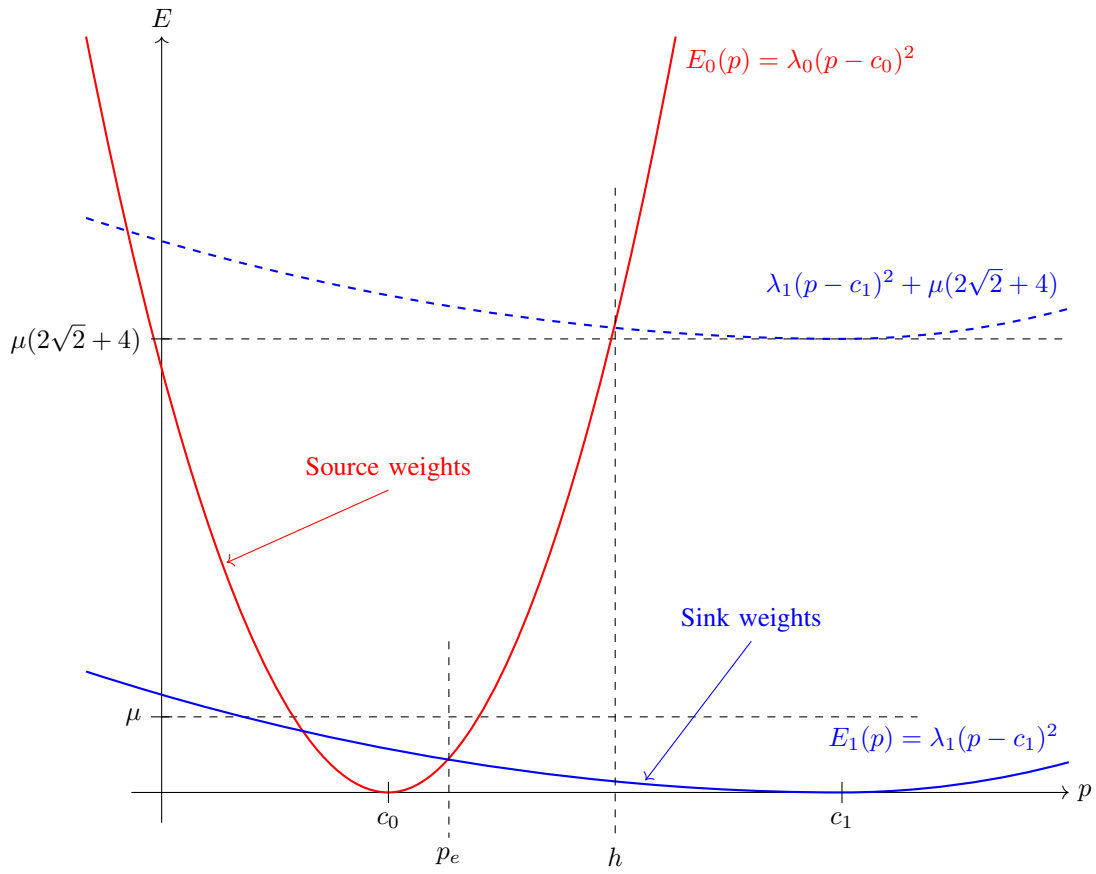


Fig. 2. Data energy functions plot.

we call  $p_e$ , i.e.  $E_0(p_e) = E_1(p_e)$ . Taking into account the relation in Equation (14), this point of zero net flow is found to be

$$p_e = c_0 + \frac{c_1 - c_0}{\sqrt{\alpha} + 1} \quad (18)$$

The point where the energies are equal,  $p_e$ , is shown in Figure 2.

We now shift our focus on the relationship between  $p_e$  and  $\alpha$ . We see that  $\alpha$  is the only tuneable parameter. From this inverse relationship we note three major points. These are

$$\begin{aligned} \text{if } \alpha = 1, p_e &= c_0 + \frac{c_1 - c_0}{1 + \sqrt{1}} = \frac{c_0 + c_1}{2} && (\text{midpoint between } c_0 \text{ and } c_1) \\ \lim_{\alpha \rightarrow \infty} p_e &= c_0 && (\text{maximum } \alpha \text{ yields lower-bound on } p_e) \\ \lim_{\alpha \rightarrow 0} p_e &= c_1 && (\text{minimum } \alpha \text{ yields upper-bound on } p_e) \end{aligned}$$

This relationship is shown graphically in Figure 3.

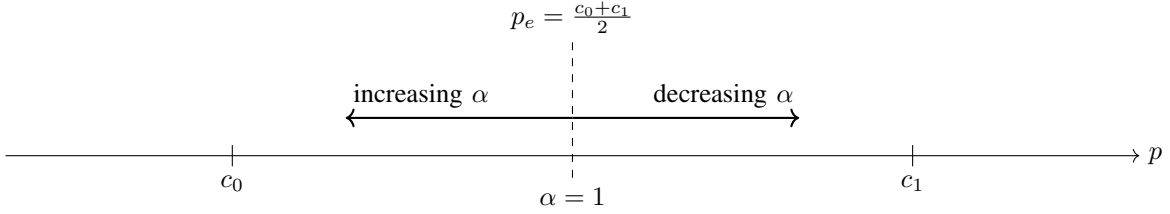


Fig. 3. Relationship between  $\alpha$  and  $p_e$ .

If we can make a good estimation for  $p_e$ ,  $c_0$  and  $c_1$  for the segmented image, then it can be shown that the corresponding  $\alpha$  can be calculated as

$$\alpha = \left( \frac{c_1 - c_0}{p_e - c_0} - 1 \right)^2 \quad (19)$$

When we calculated the intersection between the energies  $p_e$ , we ignored the other point that was out of the range  $[c_0, c_1]$ . Let this point be  $p_{e^*}$ . If this point is positive and  $0 < p_{e^*} < c_0$  then we must ensure that at no point within this range must the source flow saturate all outgoing edges. This forces a limit on how low  $\mu$  can be. This is only of significant concern when  $\alpha > 1$ . We only need to concern ourselves with the point  $p = 0$  as this is the point where the difference  $E^i(0) - E^i(1)$  is the largest. Taking into account the relation in Equation (14), the lower-bound on  $\mu$  can be shown to be

$$\mu > \frac{\lambda_1(\alpha c_0^2 - c_1^2)}{C} \quad (20)$$

We set  $C = (2\sqrt{2} + 4)$  which is the sum of all the attenuating factors of the edges connected to a node.

From Equation (16) we can see that there is a point beyond which all nodes which correspond to pixel value higher than that point will be saturated and have excess flow; this means that they will be in the source set. We will call this point the *saturation point* and denote it by  $h$ . This is shown in Figure 2. This point can be determined using

$$h = \frac{(\alpha c_0 - c_1) + \sqrt{\alpha(c_0 - c_1)^2 + \frac{C\mu}{\lambda_1}(\alpha - 1)}}{\alpha - 1} \quad (21)$$

This point is marked off in Figure 2.

Therefore, given good approximations for  $c_0$ ,  $c_1$ ,  $\alpha$ ,  $h$  and  $\mu$ , we can calculate the appropriate value for  $\lambda_1$ . This can be shown to be

$$\lambda_1 = \frac{C\mu}{\alpha(h - c_0)^2 - (h - c_1)^2} \quad (22)$$

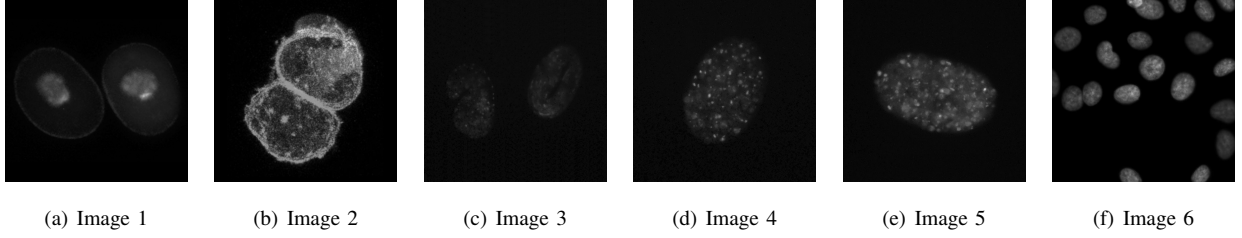


Fig. 4. Images from tuning set.

The parameter estimation is based on the assumption that sufficiently good approximations for  $c_0$ ,  $c_1$ ,  $p_e$  and  $h$  can be obtained. By sufficiently good we are referring to the closeness to the values these parameters would be for an ideal segmentation. From these approximations, we calculate  $\alpha$  using Equation (19). The parameters  $\mu$  and  $\lambda_1$  are not separable, therefore we choose to set  $\mu$ . We can then calculate  $\lambda_1$  using Equation (22). Finally  $\lambda_0$  can be calculated using Equation (14). In the next section we discuss how we make the guess for good approximations for the required parameters.

### B. Tuning the Proxy Parameters

The properties of the images obtained in fluorescence microscopy imaging can be used to guide the parameter estimation process. We focus specifically on black background fluorescent images. Due to the fact that the predominant form of noise in the imaging system is Poisson distributed, we can further assume that the darker the background, the less noise that is present therein. The Poisson process also tells us that brighter regions exhibit a greater intensity variation due to the sampling process. Therefore, the curve for  $E^i(1)$  is less convex than  $E^i(0)$  as in Figure 2 and, resultantly, the value for  $p_e$ , in Figure 3, is shifted to the left. This places a new lower-bound on  $\alpha$  for fluorescence images

$$\alpha \geq 1. \quad (23)$$

The tuning process we used is as follows: We manually segmented the fluorescent images in Figure 4. The segmentation results that were closest to the groundtruth were chosen and the corresponding proxy parameters were calculated for each image. The final setting for the proxy parameter was taken as the average value for each proxy parameter from all images.

Since the curves energy functions,  $E^i(0)$  and  $E^i(1)$ , can be tuned relative to a fixed value for  $\mu$ , which this would not impact significantly on the range of possible solution sets, we set  $\mu = 1$  in all our manual parameter tuning. We use a stopping criterion of  $\epsilon = 1 \times 10^{-3}$ . We compared the effect of using Otsu binarization, K-means ( $k = 2$ ) and Expectation-Maximisation for Gaussian Mixture Modelling (EMGMM) with ( $k = 2$ ) for generating the initial means,  $c_0$  and  $c_1$ . The values used for  $\alpha \in [1, 10, 20, 30, 40, 45, 50]$  and the values used for  $\lambda_1 \in [50, 100, 150, 200, 400, 800]$ . The remaining parameters were calculated from  $\mu$ ,  $\alpha$  and  $\lambda_1$ .

As final results we take the means of the final segmentation for the background and foreground regions. An acceptable solution was one that achieved at least 70% of the final means from the ground truth for each region. From the acceptable results, we calculate the values for  $p_e$ , Equation (18), and  $h$ , Equation (21). The means for each image can vary greatly. To put the values of  $p_e$  and  $h$  into a relative perspective, they are shown as a fraction

of the distance between  $c_0$  and  $c_1$ . Let  $k_p \in (0, 1)$  be the fraction of the distance  $p_e - c_0$  and  $c_1 - c_0$  as illustrated in Figure 5. Let  $k_h \in (k_h, 1)$  be the fraction of the distance  $h - c_0$  and  $c_1 - c_0$  as illustrated in Figure 6, we have  $0 < k_p < k_h$ .



Fig. 5.  $p_e$  as a fraction of the distance between  $c_0$  and  $c_1$ .

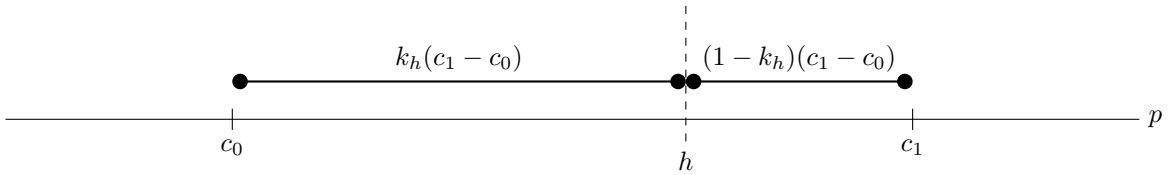


Fig. 6.  $h$  as a fraction of the distance between  $c_0$  and  $c_1$ .

Upon comparing the initial means and final means for the acceptable segmentation results, it was noted the values of the initial means are larger. This is due to over-segmentation produced by Otsu, K-means and EMGMM clustering. A naïve approach to shifting the initial means closer to the final means is to dilate the initial mask. This pushes the boundaries of the contour for the object to accept the lower intensity neighbouring pixels, as well as remove these relatively higher values from the background mask. If we are able to make a better guess to the initial means, then the fewer iterations are needed to converge within the stopping criterion.

To determine the optimal dilation size, we compare the difference of the mean values for each image, for the acceptable segmentation results only. We use an elliptical element for dilation and the size of the dilation ranged from  $r \in [1, 2, 3, 5, 7, 9]$ . A dilation size of 3 for a elliptical dilation element results in mean values that are closest to the average final means.

When defining the values for  $p_e$  and  $h$  implicitly and  $k_p$  and  $k_h$  respectively, we find the updated equation for determining  $\alpha$  is simplified to

$$\alpha = \left( \frac{1 - k_p}{k_p} \right)^2 \quad (24)$$

The weighting parameter  $\lambda_1$  can be calculated as

$$\lambda_1 = \frac{C\mu}{(c_1 - c_0)^2 \left( \left( \frac{1 - 2k_p}{k_p^2} \right) k_h^2 + 2k_h - 1 \right)} \quad (25)$$

For determining  $\alpha$  we found the average of all  $k_p$  for all acceptable segmentations. This is calculated to be

$$k_p = 0.154494.$$



From this we can calculate the value for  $\alpha$  immediately using Equation (24). This turns out to be

$$\alpha = 29.9509. \quad (26)$$

Similarly, to determine  $h$  we find the average of all  $k_h$  for all acceptable segmentations. This is calculated to be

$$k_h = 0.412737.$$

An appropriate value for  $\lambda_1$  depends on  $c_0$  and  $c_1$ , as can be seen in Equation (25), which can only be determined after the initial means are generated.

### C. Parameter Estimation Process

We now present the final parameter estimation process. The parameters whose values are fixed are

- 1)  $\mu = 1$
- 2)  $k_p = 0.154494$
- 3)  $k_h = 0.412737$
- 4)  $\alpha = 29.9509$

We first segment the image to determine the initial  $c_0$  and  $c_1$ . We can then calculate  $\lambda_1$  using Equation (25). Finally, we can calculate  $\lambda_0$  using Equation (14). The remaining parameter is the stopping criterion  $\epsilon$  which we set to  $1 \times 10^{-3}$ .

## V. EXPERIMENTAL RESULTS

We compare our results to two previously published parameter settings. Their results showed excellent segmentation output on synthetic images and mammography images with very high robustness against noise. They do not specify the noise type. Their parameter setting was based on a time-lapse series of fluorescence images. Their scheme is a hybrid of algorithms designed to segment whole fluorescent cells; however, we use the parameter setting they have presented for segmentation only. Their parameter setting was obtained by minimising the Jaccard coefficient over the time-lapse series.

To generate the initial means we used the EMGMM with  $k = 2$  which was followed by an elliptical dilation of size 3. The results of all segmentation scheme are shown from Figure 7 to Figure 21.

In Table I, which compares the segmentation efficiency of each method, we differentiate between methods on the same image as follows:

**[imageno]-[method],**

where *imageno* goes from 1 to 25 and *method* is defined as follows:

- n** - using parameter setting presented by El-Zehiry *et. al*
- m** - using parameter setting presented by Masaka *et. al*
- d** - Proposed method with parameters estimated from an initial EMGMM segmentation with  $k = 2$  and an elliptical dilation of  $3px$ .

In Table I we compare the accuracy and MCC of each segmented result for each scheme. Accuracy is the fraction of the pixels that are correctly classified from among all pixels. MCC is the *Matthews Correlation Coefficient* and is a more accurate measure of accuracy when comparing classes whose sizes differ greatly.

We used a 8-connected graph for all methods.

TABLE I: Segmentation Efficiency.

Image	El-Zehiry <i>et. al</i>		Masaka <i>et. al</i>		Proposed	
	Accuracy	MCC	Accuracy	MCC	Accuracy	MCC
1	0.770111	0.626140	0.967117	0.934010	0.959427	0.919468
2	0.747253	0.416180	0.335449	-0.008374	0.862671	0.748686
5	0.912262	0.811918	0.851883	0.739708	0.916992	0.842769
6	0.515686	0.300907	0.603195	0.028915	0.966156	0.931253
9	0.886490	0.589732	0.938583	0.834732	0.990768	0.970635
12	0.806732	0.519903	0.309845	0.060018	0.905685	0.808358
15	0.962357	0.507270	0.098129	0.051537	0.990158	0.911074
17	0.888229	0.452365	0.150055	0.020336	0.915009	0.733933
18	0.595612	0.384991	0.567032	NaN	0.960739	0.922580
19	0.852585	0.559970	0.570099	0.393942	0.975266	0.933388
20	0.914856	0.719637	0.679703	0.479944	0.966690	0.904878
21	0.913818	0.678954	0.181793	0.035231	0.967438	0.885155
22	0.703156	0.469557	0.449310	NaN	0.981735	0.963345
24	0.921356	0.562635	0.136047	0.047223	0.882690	0.661018
25	0.573715	0.296608	0.511276	NaN	0.959915	0.920148

TABLE II: Overall Segmentation Efficiency.

Method	Accuracy	
	Mean	Std. Dev
El-Zehiry <i>et al.</i>	0.805732	0.151199
Maska <i>et al.</i>	0.547369	0.321099
Proposed	0.935329	0.064493

The general parameter settings by El-Zehiry *et al.* clearly outperform by the parameter settings presented by Masaka *et al.* by a 25.8363% difference in accuracy. However, the proposed method boasts an increase of 12.9597% above El-Zehiry's parameter settings. The proposed method is also much more stable over a greater variety of fluorescence images, as can be seen by the standard deviation of accuracy shown in Table II.

## VI. CONCLUSION

Fluorescence images are hugely diverse; even so of the images within the fields of cellular biology and medicine. The design of a general and automatic segmentation method is not a trivial exercise; and, it is much needed.

We have presented a novel parameter estimation technique which is able to tune the parameters of the graph-cut application of the Chan-Vese segmentation method, to the specific image. This is a huge contrast in comparison to

the fixed parameter settings proposed by El-Zehiry *et al.* and Masaka *et al.* Our method, does however, rely on the strong assumption that the initial means obtained from the initial unsupervised segmentation scheme is relatively close to the final means. Fortunately though, in the domain of biological and medical fluorescence images, the unsupervised segmentation results obtained from an Otsu, K-means or EMGMM clustering is close enough to outperform the competitor parameter settings. We have shown that an EMGMM clustering and a dilation of 3 pixels, with an elliptical dilation element, provides the best approximation to the final means which results in an average of 93.5329% classification accuracy. Given the diversity of fluorescence images in the test set, this is a very pleasing result, especially when compared to the competitor parameter settings by El-Zehiry *et al.* which showed an average of 80.5732% and Masaka *et al.* which showed an average of 54.7369%.

Once the initial means have been obtained, the parameters are adapted to the image by direct calculation by means of the *relationship variables and formulae*. These relationship variables and formulae encode the important relation of the parameters with each other. This allows the ability to adapt the parameter settings according to the properties of the image. These resulting parameters only allow high segmentation accuracy if the image has the properties that are encoded in the relationship variables and formulae.

The relationship formulae only take into account the information from the intensity of the image. Other information, such as texture, can be incorporated into the formulae as well. This will include adapting the graph to hold this information so that it can be accounted for in the energy function.

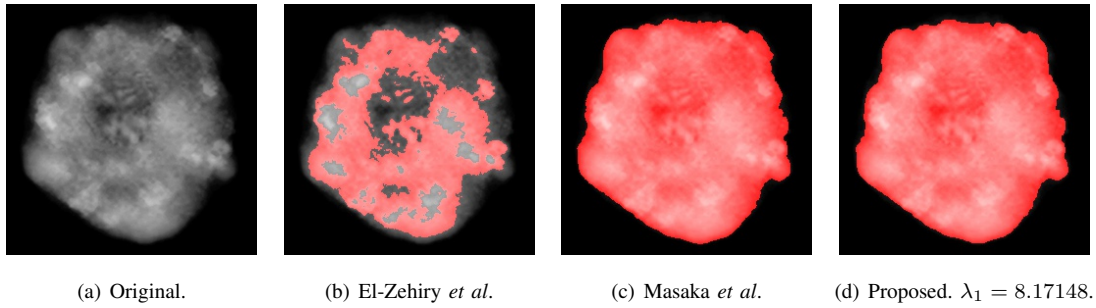


Fig. 7. Image 1 from test set segmentation results.

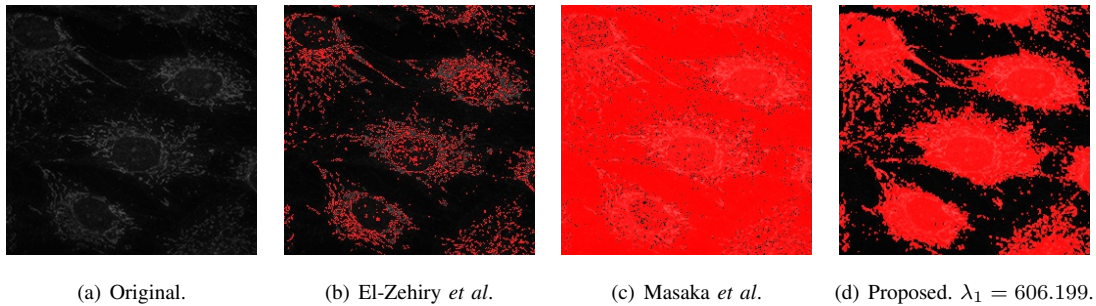


Fig. 8. Image 2 from test set segmentation results.

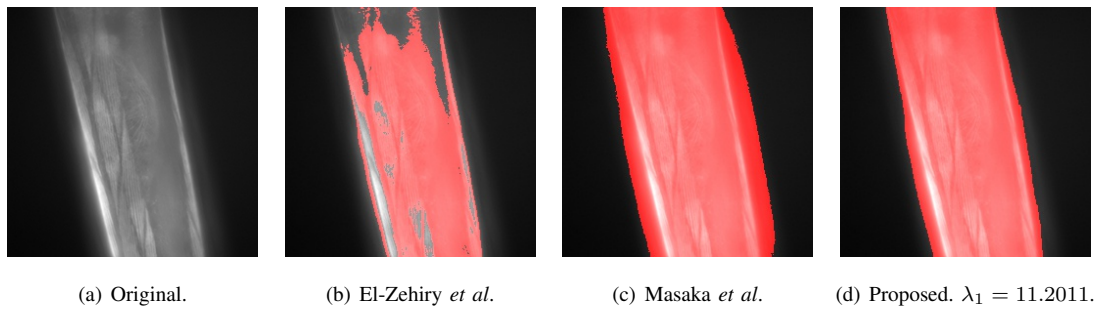


Fig. 9. Image 5 from test set segmentation results.

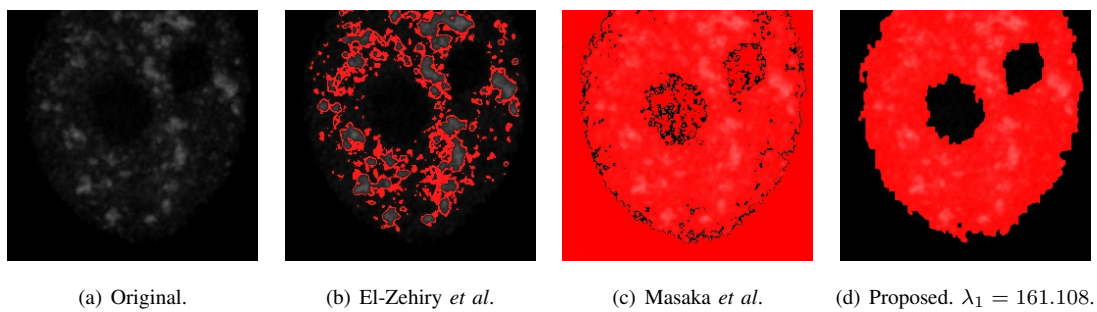


Fig. 10. Image 6 from test set segmentation results.

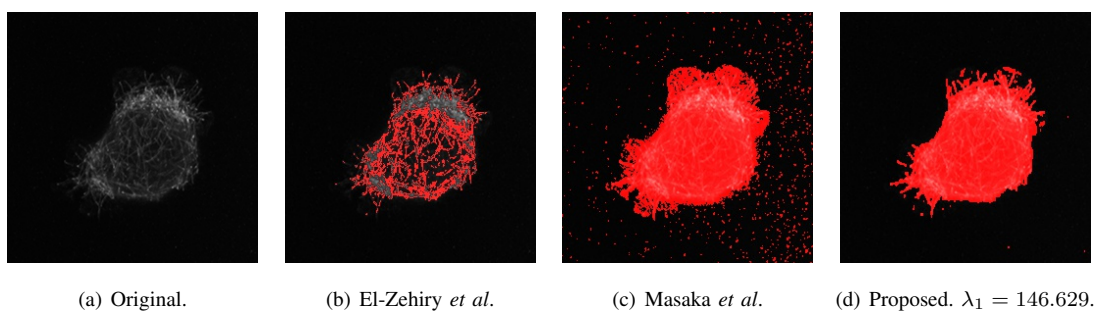


Fig. 11. Image 9 from test set segmentation results.

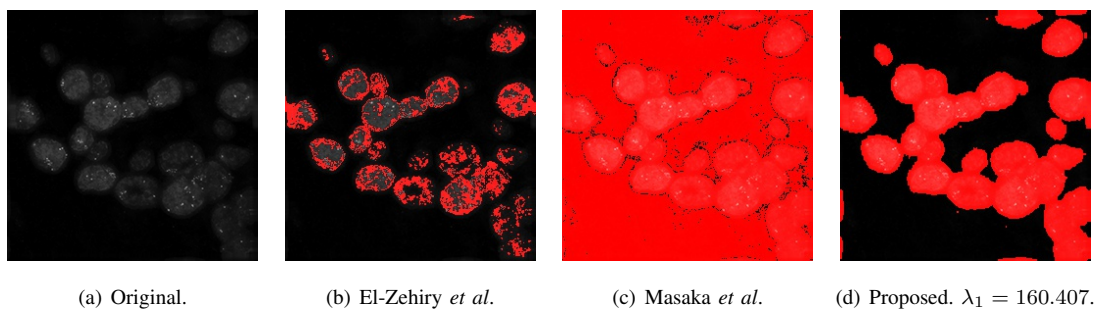


Fig. 12. Image 12 from test set segmentation results.

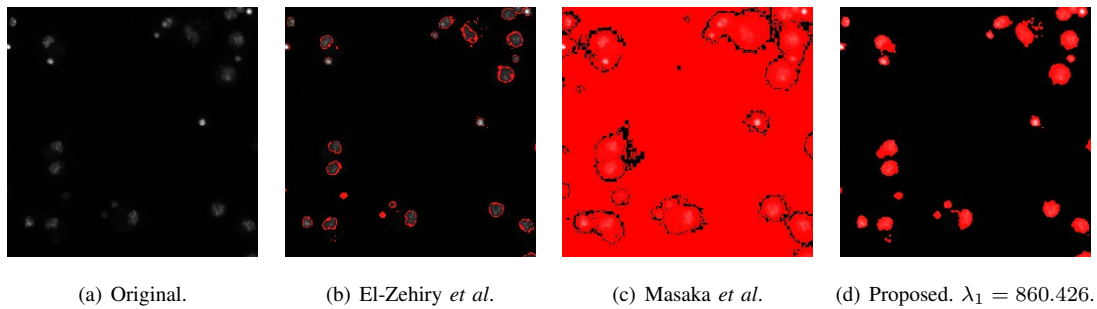


Fig. 13. Image 15 from test set segmentation results.

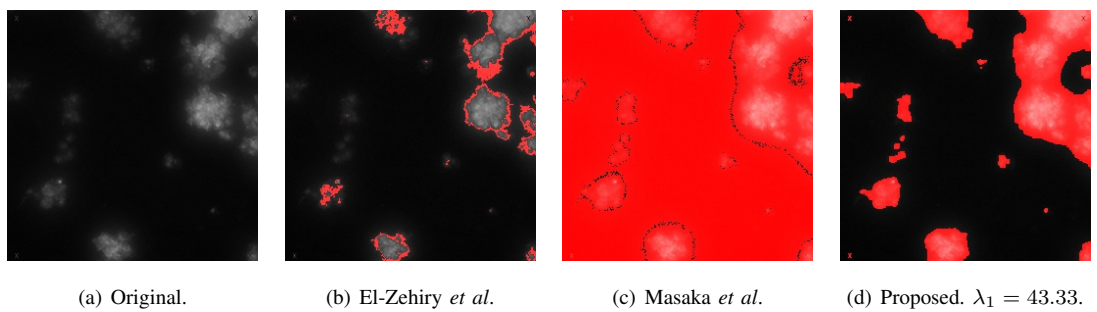


Fig. 14. Image 17 from test set segmentation results.

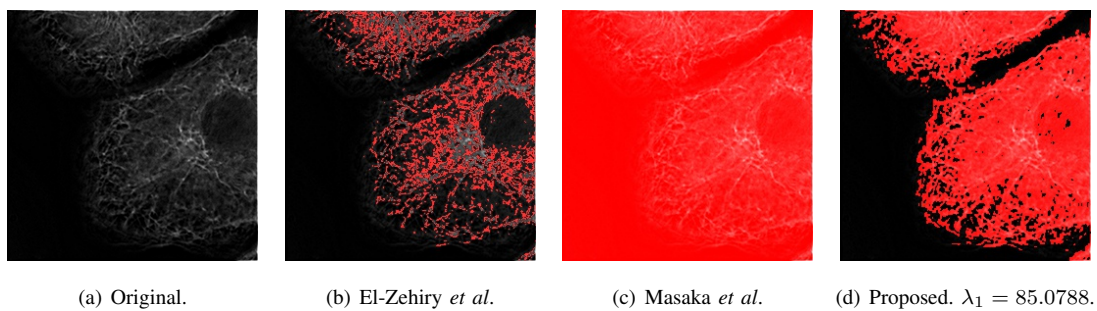


Fig. 15. Image 18 from test set segmentation results.

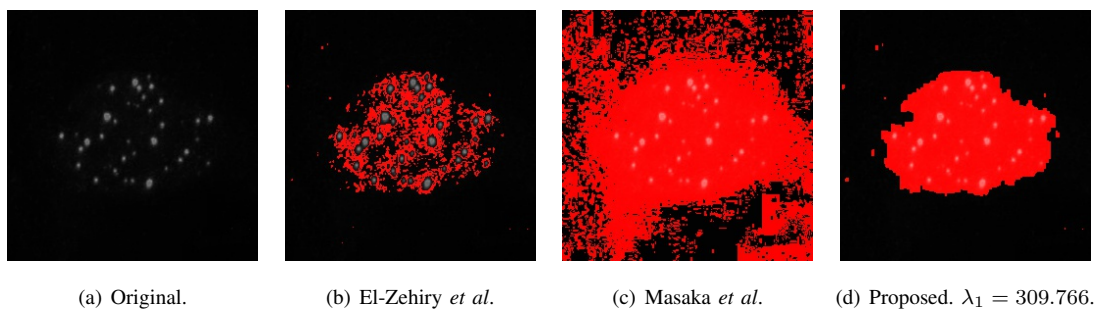


Fig. 16. Image 19 from test set segmentation results.



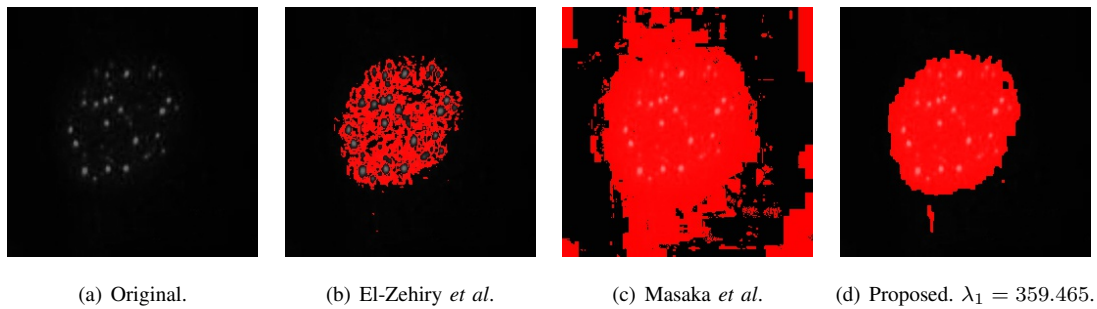


Fig. 17. Image 20 from test set segmentation results.

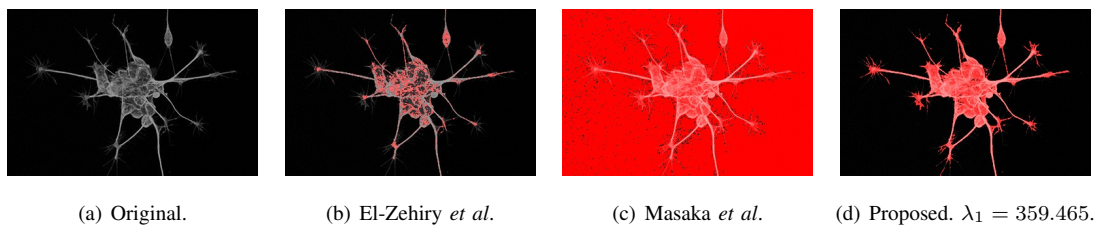


Fig. 18. Image 21 from test set segmentation results.

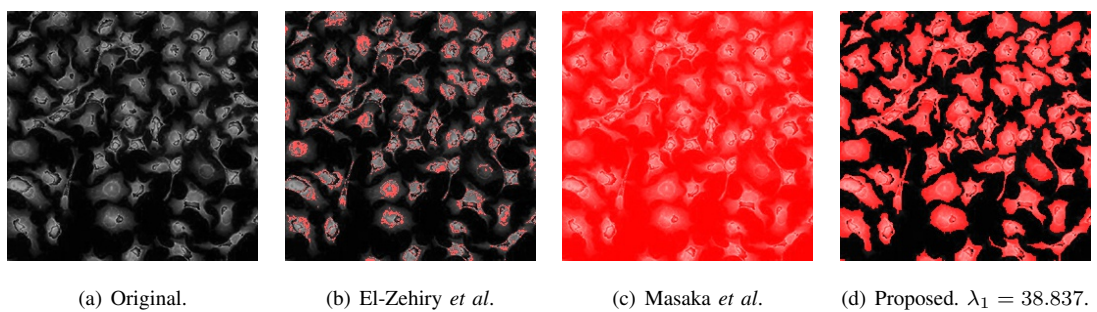


Fig. 19. Image 22 from test set segmentation results.

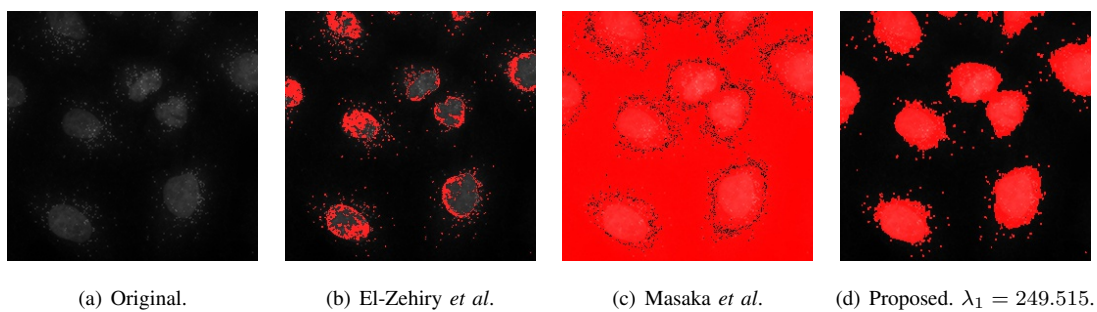


Fig. 20. Image 24 from test set segmentation results.

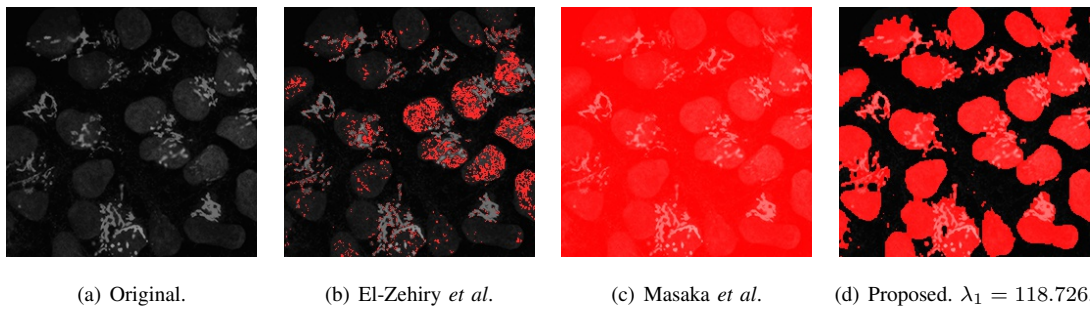


Fig. 21. Image 25 from test set segmentation results.

## REFERENCES

- [1] H. Kopka and P. W. Daly, *A Guide to L<sup>A</sup>T<sub>E</sub>X*, 3rd ed. Harlow, England: Addison-Wesley, 1999.